Observations of the stress developed in Si inclusions following plastic flow in the matrix of an Al–Si–Mg alloy

Davidson, CJ, Finlayson, TR, Fitzpatrick, ME, Griffiths, JR, Oliver, EC & Wang, Q

Original citation & hyperlink:
Davidson, CJ, Finlayson, TR, Fitzpatrick, ME, Griffiths, JR, Oliver, EC & Wang, Q 2017, 'Observations of the stress developed in Si inclusions following plastic flow in the matrix of an Al–Si–Mg alloy' *Philosophical Magazine*, vol 97, no. 17, pp. 1398-1417
http://dx.doi.org/10.1080/14786435.2017.1296978

DOI 10.1080/14786435.2017.1296978
ISSN 1478-6435
ESSN 1478-6443

Publisher: Taylor and Francis

This is an Accepted Manuscript of an article published by Taylor & Francis in Philosophical Magazine on 10th April 2017, available online: http://www.tandfonline.com/10.1080/14786435.2017.1296978

Observations of the stress developed in Si inclusions following plastic flow in the matrix of an Al-Si-Mg alloy

Cameron J. Davidson[a*], Trevor R. Finlayson[b], Michael E. Fitzpatrick[c], John R. Griffiths[d], Edward C. Oliver[e] and Qigui Wang[f]

[a] *CSIRO Energy, PO Box 883, Kenmore, QLD 4069, Australia*

[b] *School of Physics, University of Melbourne, VIC 3010, Australia*

[c] *Centre for Manufacturing and Materials Engineering, Coventry University, Coventry, CV1 5FB, UK*

[d] *CSIRO Mineral Resources, PO Box 883, Kenmore, QLD 4069, Australia*

[e] *CCLRC Rutherford Appleton Laboratory, Chilton, Didcot, OX11 0QX, UK*

[f] *General Motors, Global Propulsion Systems, 800 North Glenwood Ave, Pontiac, MI 48340-2920, USA*

* Corresponding author:
CSIRO Energy, PO Box 883, Kenmore, QLD 4069**,** Australia
cameron.davidson@csiro.au

Abstract

Measurements are made of the stress developed in near-spherical elastic inclusions in an elastic plastic matrix under both tension and compression loading. Two experimental conditions are reported. The first case is where no thermal mismatch exists between the inclusions and the matrix, so that the stress in the inclusion is purely a result of the misfit in the elastic moduli and of the distortion of the plastic slip-line field around the inclusion. The observations are believed to be the first such and are in qualitative agreement with finite element modelling for idealised inclusion distributions. The second case is the more usual one where a thermal misfit stress exists and observations are reported of the stress relief effects caused by the interaction of the plasticity-induced stress with the thermal and elastic misfit stresses.

Keywords: residual stress relaxation, plasticity of metals, residual stress, neutron diffraction, aluminium alloys, composite materials, plastic misfit stress.

1. Introduction

Stresses in the inclusions of two-phase composites are caused by differences between the thermal expansion coefficients and the elastic moduli of the matrix and inclusions and by stresses associated with the deformed slip-line field in the plastic matrix. These three components of stress are denoted respectively as σ^{th}, σ^{el} and σ^{pl}. Observations of these stresses are commonly made by X-ray or neutron diffraction, and while there have been many direct observations, measurements and calculations of the first two components, the same is not true for the plasticity stress, σ^{pl}. This is because, as is well known (e.g. [1]), plastic flow in the matrix has two simultaneous effects.

The main effect is that plastic flow in the matrix alters the shape misfit stress fields. In a homogeneous material plastic flow will remove residual stresses, as in the stretching of aluminium plates after heat -treatment, whilst the presence of inclusions means that, after plasticity, a shape misfit will still be present but now it has a plastic rather than a thermal origin. The degree to which the pre-existing thermal misfit is offset will depend on the level of the plastic strain, usually being complete at strains of a few percent [2]. The effect of plasticity on relieving a residual stress is non-polar: that is, it is the same after either tensile or compressive plastic flow.

The second effect, and the one causing a plasticity stress, is that the plastic strain introduces a hydrostatic component of stress into the matrix because of the distortion of the plastic slip-line field [3,4,5] and this increases the stress in the inclusion: the effect is polar so that compression straining produces more compression in the inclusion and tensile straining produces more tension. As with stress relief, the plasticity stress reaches an asymptotic value: once the slip-line field is fully established, usually after a few percent strain, the plastic constraint factor is constant. Confirmation of the plasticity stress has been made by many authors applying both analytical and numerical methods (see the review by Benzerga and Leblond [6]). However, separating the two effects (stress relief and plasticity stress) is not straightforward and experimental observations of the plasticity stress have so far only been indirect.

Most measurements of the stress in composites have been made with synthetic composites such as aluminium alloy reinforced with SiC, TiC or Al_2O_3. There have been fewer experiments using natural composites such as that used in this research, the Sr-modified aluminium casting alloy Al-7Si-0.4Mg. Few measurements [7,8,9] have

been made on this alloy despite its commercial importance and, particularly, the fact that fracture initiates at the eutectic Si inclusions [10,11,12]. Further, in two of these cases [7,8] observations could only be made at the surface because of the techniques used (laboratory X-ray diffraction and Raman spectroscopy). In the third case [9] synchrotron X-ray radiation was used to sample the entire volume of the specimen but measurements were limited to very small applied strains. We have previously reported results of an experiment that avoided these problems by using neutron diffraction to measure the development of stresses in the Si inclusions while tensile samples were loaded in a neutron beam [13]. However, only the total stress in the Si inclusions could be measured, and the separate contributions referred to above were not identified.

The aluminium alloy used in this study offers an advantage not available in most natural composites: the reinforcing second phase is pure Si and so it is easy to obtain the stress-free lattice parameter for subsequent calculations of strain, a problem that has frustrated others [14,15,16,17].

In this paper we report an experiment in which the complicating effect of the initial thermal stress is avoided by carrying out a cyclic tension/compression test at a temperature where σ^{th} is zero. This has allowed us to measure σ^{pl} unambiguously as a function of the applied plastic strain. We have complemented this experiment with one at room temperature where σ^{th} is significant.

2. Materials and methods

2.1 Materials

The material was alloy A356, with Sr added to spheroidise the eutectic Si inclusions. The composition was (wt%): 6.6 Si, 0.4 Mg, 0.05 Fe, 0.18 Ti, 0.019 Sr with Cu, Mn, Zn all <0.01, balance Al. Plates, measuring 140 × 160 × 25 mm^3, were made by sand-casting. The plates were hot-isostatically pressed for 2 hours at 525°C and 103 MPa to eliminate essentially all the porosity. Slices 25 mm wide were cut from the plates and were solution heat-treated at 540°C for 6 hours followed by a cold water quench and ageing at 170°C for 6 hours.

The microstructure has been described previously [18,19,20]. It is highly non-uniform, comprising (i) dendrite colonies (grains) some 0.8 mm in diameter, (ii)

dendrites with a secondary dendrite arm spacing of ~60 μm, and (iii) inter-dendritic eutectic Si inclusions with a volume-equivalent diameter of ~3 μm and an aspect ratio of ~1.6 [21] together with age-hardening nano-precipitates of MgSi. The volume fraction of the Si inclusions is 0.062.

[Table 1 near here]

We assume that the aluminium matrix and silicon inclusions are elastically isotropic with elastic constants and thermal properties as given in **Error! Reference source not found.**. Isotropic elastic constants are derived from the single crystal values using the method of Gnäupel-Herold [22]: single crystal values for Al and Si are from [23] and [24] respectively and the coefficients of thermal expansion are from [25] and [24]. The temperatures quoted in the Table are those used in the experiment described in §3. The yield strength was 279 MPa at 20°C and 247 MPa at 130°C.

2.2 Mechanical tests

Tests were carried out on a servo-hydraulic Instron *in situ* at the ENGIN-X beamline of the UK's ISIS pulsed neutron source [26]. The experimental set-up is shown schematically in Figure 1. Cylindrical test specimens were machined from the heat-treated slices. They were gripped in split collets, the button-ends allowing tension/compression cyclic testing with no backlash as the load is reversed. The gauge dimensions (22 mm length and 10 mm diameter) were chosen to prevent plastic buckling in compression, based on the measured rates of work-hardening [27]. The applied strain was measured by an extensometer mounted on the gauge section.

Testing was carried out in steps with the Instron driven at a constant crosshead speed to pre-determined stresses (for stresses below yield) or strains (for stresses above yield). Once the specimens had yielded, the plastic strain rates during loading were between 7 and 25 x 10^{-5} s^{-1}. At each step, control was switched to constant strain to allow diffraction patterns to be collected, using count times of 20 minutes. Once the specimens had yielded, stress relaxation occurred and the definition of the effective stress, applicable to each strain increment is described in §4.

Testing was performed at 20°C and 130°C, the higher temperature being chosen because the compressive thermal stress which is present in the inclusions at 20°C is calculated to vanish at 130°C (it then becomes tensile at higher temperatures).

2.3 Neutron diffraction

The ENGIN-X instrument has two fixed-angle detector banks centred on scattering angles of ±90°, (Figure 1). The detectors measure time-resolved diffraction patterns corresponding to scattering vectors aligned at ±45° to the incident beam with a timing window set to detect inter-planar spacings in the range 0.076 nm $\leq d_{hkl} \leq$ 0.24 nm. The load axis was aligned at 45° to the incident beam, parallel to the scattering vector for the "Bank 1" detector which, therefore, for a sample under an applied load, will record the lattice spacings parallel to the applied load. At the same time, the "Bank 2" detector will record the lattice spacings in the transverse direction. The volume of material irradiated by the neutron beam was $4 \times 4 \times 8$ mm^3. Diffraction patterns from the two detectors are shown in Figure 2. The diffraction patterns were analysed by Rietveld refinement of the complete range of *d*-spacings using the software of Larson and Von Dreele [28].

Before starting the experiment, the "Bank 1" and "Bank 2" detectors were calibrated by following the standard procedure of measuring lattice spacings of a NIST standard CeO_2 powder. A reference value of the strain-free lattice parameter, a_0, for Si was determined by analysing a NIST standard Si powder, noting that the inclusions in the alloy are also pure Si. The results are shown in **Error! Reference source not found.**. Despite the CeO_2 calibration, "Bank 2" consistently gave a value of a_0 some 0.01% larger than that from "Bank 1". When calculating strain values in the Si inclusions during the experiment, the strain-free values of a_0 were those recorded in **Error! Reference source not found.** for each Bank.

[Table 2 near here]

It was not practicable to make the corresponding a_0 calibration for the Al dendrites. This is because they contain, in solution, Mg and Si as well as impurity elements, all of which affect the lattice parameter [29], and producing a stress-free powder from the alloy would require separating the Al matrix from the micron-sized Si inclusions, a problem noted by others (see, e.g., [30]). Requena *et al.* [31] show that the problem of an unknown a_0 is avoided by only calculating the deviatoric stresses, but calculating the complete stress tensor, including the hydrostatic and deviatoric components, is outside the scope of the present paper.

3. Results I: thermal misfit stresses

3.1 Thermal misfit stresses in Si at 20°C

Thermal misfit stresses exist in both the Si inclusions and the Al matrix as a result of their thermal expansion mismatch. The stresses in the Si inclusions are homogeneous (at least, for spherical inclusions). Diffraction patterns were collected from a tensile test specimen resting on the sample table under zero applied stress. To check that the stress in the inclusions was hydrostatic and unaffected by orientation in the tensile gauge section, diffraction patterns were collected with the specimen oriented both vertically and horizontally with respect to the table.

No effect of orientation was detected, confirming that the stress is indeed hydrostatic. The three specimens used in this research gave values of −145±2, −155±1 and −170±2 MPa. The mean value, −157 MPa, is consistent with that reported by us in an earlier experiment [13]; the variation in the means of the three measurements of ±12 MPa is greater than the counting error and represents the probable uncertainty in the stress data reported in the present paper.

3.2 Thermal misfit stresses in Si at elevated temperature

When the specimen is heated, the stress in the Si inclusions becomes less negative because Al expands more than Si. Diffraction patterns were collected while the specimen was heated and the results are shown in **Error! Reference source not found.**. The "Measured stress" values are calculated from the measured strains and the elastic constants for the particular temperatures listed in **Error! Reference source not found.**. The "Calculated stress" values are those predicted by the Eshelby method [32] assuming the 20°C value of −155 MPa found for this particular specimen and then using mean values of the temperature-dependent coefficients of thermal expansion for Al and Si. The agreement of experiment with theory is excellent, **Error! Reference source not found.**. The thermal stress is negligible at 130°C, and this result is used for the experiment reported in the following section.

[Table 3 near here]

4. Results II: strain-cycling tests

Only one test was conducted at 130°C: this was a tensile strain of 0.02 followed by a compression strain of 0.02. The strains were defined from the initial zero for the extensometer and this meant that the reverse strain was roughly twice the forward strain (Figure 3). At the start of the test the temperature was 127°C and by the end it had risen to 134°C. Three thermocouples were spot-welded along the gauge length and the temperature differences were less than 5°C. We therefore report this test as 130±4°C.

A further two tests were performed at 20°C. The first was the application of a tensile strain of 0.02 followed by a compression strain of 0.02; the second was the reverse, a compression strain of 0.02 followed by a tensile strain of 0.02. As with the 130°C test, the reverse strains were roughly twice the forward ones.

As noted in §2.2, diffraction data were collected at constant strain and, once yield was exceeded, stress relaxation occurred. The amount of relaxation increased with increasing applied strain and reached a maximum of about 70 MPa for the 130°C test and 55 MPa for the 20°C tests. Stress relaxation has two consequences: (i) since "constant strain" means constant total strain, the plastic strain increased by an amount equal and opposite to the relaxation in elastic strain; and (ii) it becomes necessary to define the effective stress associated with each strain increment. The first question is straightforward: the maximum elastic strain relaxation is ~0.001 at a plastic strain of ~0.03 so the effect is negligible. The second question is answered in the following way. The applied stress was recorded every 3 to 5 seconds during the 20 minutes required for an adequate number of counts. We define the mean stress, σ^*, given by:

$$\sigma^* = \frac{1}{t_f}\sum_0^{t_f} \sigma(t).\delta t \qquad (1)$$

in which counting started at $t = 0$ and ended at $t_f = 20$ minutes.

The stress/strain data from the Instron load frame are shown in Figure 3. Figure 3(a) includes, as an example, the maximum (initial), minimum (final) and mean stresses for each strain increment. The mean stress, σ^*, was only slightly greater than the stress at the end of the 20 minute data collection period, (between 0 and 5 MPa, as the plastic strain increased from zero to its maximum of ~0.03). Accordingly, in what follows we

write $\sigma^{app} = \sigma^*$ for the applied stress. At time, t^*, $\sigma^{app} = \sigma^*$ and t^* was between 0.3 and 0.4 of the total time (i.e. between 6 and 8 minutes).

The variation of strain, ε^i, in the Si inclusions with σ^{app} and the corresponding inclusion stresses, σ^i, are shown in Figures 4 to 6. The slopes of the elastic parts of the loading, unloading and re-loading curves for the two room temperature tests provide six measures of $d\sigma^i/d\sigma^{app}$; these give a mean value of 1.24 MPa/MPa. Eshelby theory [32] predicts 1.32 MPa/MPa for 6 vol% spherical inclusions. The corresponding prediction at 130°C is 1.34 MPa/MPa reflecting the proportionally greater decrease in Young's modulus of the Al matrix compared to that of the Si; the measured values had a mean of 1.15 MPa/MPa which is a discrepancy beyond that attributable to experimental scatter. One reason for the poor agreement between theory and measurements could be localised relaxation in the matrix immediately surrounding the inclusions. This is not detectable in the bulk stress and strain measurements.

5. Discussion

5.1 Measurements at 130°C

The aim of this research was, first, to identify and measure the plasticity stress, σ^{pl}, and second, to comment on its interaction with the initial thermal stress, σ^{th}. This second case is discussed in §5.3.

Error! Reference source not found. and Figure 4(b) show that the Si inclusions have no initial thermal misfit stress at 130°C, thus eliminating any complications arising from it. Further, Figure 3(a) shows that, at 130°C, the alloy is effectively elastic – perfectly plastic in the initial tensile part of the loading cycle although in the subsequent compression part of the cycle the Bauschinger effect means that plastic flow occurs under an increasing stress. Reflecting these stress/strain relationships, Figure 4(b) shows that, in tension, the inclusion stress increases (becomes more tensile) under a constant applied stress once the yield stress is reached whilst in compression it increases (becomes more compressive) under an increasing applied stress. The plasticity stress, σ^{pl}, is the difference between the total stress in the inclusion and the stress expected from elasticity theory as denoted by the dashed lines in Figure 4(b). The sense of σ^{pl} is the same as that of the applied stress: during tensile loading σ^{pl}

becomes increasingly tensile while in compression it becomes increasingly compressive. The variation of σ^{pl} with the applied plastic strain for both the tensile and compressive parts of the cycle is shown in Figure 7 together with the results of modelling described in §5.2.

The measurements of σ^{pl} during tensile loading are, to our knowledge, the first made without any complicating effects of an initial thermal stress. The effects seen on the subsequent compression part of the load cycle are not entirely clear-cut because the inclusions presumably have some residual stress following the tension cycle, although Figure 4(b) suggests that this was very small. Unfortunately, time constraints meant that a second, "compression-first" experiment could not be done. Nevertheless, Figure 7 shows that there is a remarkably similar response in both tension and compression.

5.2 Theoretical models for σ^{pl}

As noted in the Introduction, several models have been proposed for the development of σ^{pl}. Here we discuss two of them. The first is that of Ashby [33] and of Brown and Stobbs [34,35] which was developed by Brechet *et al.* [36] for the SiC inclusions in an Al-SiC composite and by Cáceres and Griffiths [37] for the Si inclusions in the same Al-Si-Mg alloy as used in the present work. The model predicts that σ^{pl} should increase linearly with plastic strain until a certain strain, ε^*, after which it varies as its square root. Cáceres and Griffiths concluded that the stress in the Si inclusions at a plastic strain of 0.03 was about 780 MPa, or three times the yield strength of the alloy. This figure was justified on the basis of the statistics of inclusion cracking and on the rate of work-hardening (attributed to the back-stress exerted by the inclusions). However, their value is far greater than that shown in Figure 7 and greater than found in earlier experiments [7,8,13] and we conclude that the model is inapplicable to the inclusions dealt with in this research.

An alternative approach is to use finite element methods. As noted by Barnett *et al.* [38], many, if not most, such reports deal only with the stresses at the inclusion/matrix interface rather than with the volume average inclusion stress which is the only one accessible to presently available experimental techniques. Early results on the volume average stress using finite element modelling [39] showed no evidence of a

plasticity stress, the stress in the inclusion being directly proportional to the applied stress. However, the existence of a plasticity stress is implicit in the later work of Segurado and LLorca [40] as shown in Figure 8 for a low yield strength Al alloy (0.2% proof stress of 157 MPa) reinforced with SiC inclusions. When the applied stress is below yield, the stress in the SiC inclusions is about 1.5 times the applied stress, consistent with classical elasticity [32] but, as plastic flow develops, the stress in the inclusions increases at a higher rate. The plasticity stress is the difference between the total stress and the extrapolated elastic stress, Figure 8(b), and it increases rapidly at first but then more slowly, well below the rate expected for a parabolic dependence [33]. The result that the plasticity stress approaches an asymptotic multiple of the matrix yield stress is consistent with previous work (see, e.g., [5,41,42]) and, in particular, with the interpretation that it is a result of plastic constraint in the matrix.

The data in Figure 8 are qualitatively consistent with those in Figure 7, notwithstanding the differences in properties of both matrix and inclusion between the model and our experimental alloy. Running the model with the appropriate material properties will not affect these qualitative conclusions. Further, the distribution of Si inclusions in our experiment is highly non-uniform, being confined to the inter-dendritic regions of the microstructure, and we judged that the effort of modelling such a microstructure in detail could not be justified.

5.3 Effects of plastic strain in the presence of an initial thermal stress

Figure 7 shows that at 130°C, when there is no thermal residual stress, σ^{pl} has the same sense as the applied stress, positive during tension and negative during compression. The situation is complicated at 20°C because the development of σ^{pl} occurs simultaneously with the relief of the initial compressive thermal stress. The experiments only measure the deviation of the inclusion stress from the elastic loading line and therefore record an *apparent* plasticity stress. For the tension-first test at 20°C, Figure 5(b), the apparent plasticity stress is greater in the initial tension part of the cycle than in the subsequent compression part although in both cases the deviation is in the same sense as the applied stress. For the compression-first test, Figure 6(b), the deviation is greater during the initial compression than in the subsequent tension part of the cycle but, strikingly, it is positive in both parts of the cycle. The apparent plasticity

stresses for the two experiments are shown in Figure 9, together with the lines derived from the modelling of Segurado and LLorca [40].

In the tension-first experiment, Figure 9(a), the large apparent plasticity stress in the initial tension part of the cycle is because the true plasticity stress is enhanced by the simultaneous relaxation of the thermal stress. In the subsequent compression part of the cycle most or all of the thermal stress has been relaxed by the tensile pre-strain and so the apparent plasticity stress is mostly due to the true (compressive) plasticity stress. By contrast, in the compression-first test, Figure 9(b), the apparent plasticity stress in the initial compression part of the cycle is due to relief of the large initial thermal misfit stress opposed by the relatively small compressive plasticity stress. When the specimen is re-loaded in tension the initial thermal stress has been relaxed by the pre-strain and the positive deviation from the elastic loading line is mostly due to the plasticity stress and conforms to the predictions of the model.

Similar tension/compression asymmetry effects have been reported by others [30,43,44] and attempts to model the interaction of the stress relief effect with the plasticity stress effect include those of Roatta and Bolmaro [45] and, more recently, of Zhang *et al.* [46]. Levy-Tubiana *et al.* [47] made detailed observations of the interaction between an initial thermal stress with an applied plastic strain and their modelling showed the short-comings of linear superposition. Unfortunately, it has not been possible to apply the methods of Zhang *et al*. [46] to our experiments and we are unaware of other, more suitable, models.

5.4 Implications for the fracture of the Si inclusions

As noted in the Introduction, fracture in these alloys initiates by brittle fracture of the elastic Si inclusions, starting at applied tensile strains of about 0.02. Our results, Figure 5(b), show, therefore, that the fracture strength of the particles is ~400 MPa, a figure consistent with previous work [7,8]. If a fracture surface energy of $2\gamma = 2.5$ J/m^2 [48] is assumed, this fracture strength is consistent with a surface crack or defect of length of ~1μm. Such large defects are unlikely in the present case and an explanation for the fracture of the inclusions will have to include local stress concentration effects such as dislocation pile-ups in the aluminium matrix. Unfortunately, such localised stress concentrations are not detectable by the diffraction techniques used here which

only measure the volume average stress. An alternative view, not requiring stress concentrations, is that of Campbell [49] who proposes that Si eutectic inclusions are intrinsically weak by virtue of folded oxide films embedded in the inclusions, although evidence for such films is yet to be found [50].

6. Conclusions

(1) This paper reports the first direct measure of the plasticity stress in second-phase inclusions of a composite. This was achieved by carrying out experiments at an elevated temperature, 130°C, where the inclusions were free of an initial thermal stress.

(2) At 130°C, the absence of the thermal stress means that there is symmetry in the magnitude of plasticity stress generated, irrespective of whether deformation is tensile or compressive. The magnitude of the plasticity stress approaches 90 MPa for an applied total strain of 0.03.

(3) Following from (1), the paper reports the way in which plastic flow modifies the thermal stress in the inclusions of a composite when such thermal stresses exist. Experiments were performed at both room temperature (where there is a thermal stress) and at 130°C (where the thermal stress is absent).

(4) We demonstrate that measurements at room temperature are ineffective in determining the plasticity stress because the relaxation of the thermal misfit stress is overlaid on the plasticity effect.

(5) It is shown that the low fracture strength of the eutectic Si inclusions implies that localised high stress concentrations are present that are not detectable by the experimental technique used here. An alternative explanation is that the inclusions are weakened by the presence of incorporated oxide films.

Acknowledgements

We are grateful to the CCLRC for the provision of beamtime at the ISIS neutron facility and to General Motors R&D for making the cast plates. Professor Phillip Withers made helpful comments on the manuscript.

Funding

CJD, TRF, JRG acknowledge support from the Access to Major Research Facilities Programme, a component of the International Science Linkages Programme established under the Australian Government's innovation statement, Backing Australia's Ability, [Proposal Number 07/08-N-21].

MEF is grateful for funding from the Lloyd’s Register Foundation, a charitable foundation helping to protect life and property by supporting engineering-related education, public engagement and the application of research.

References

[1] S.M. Pickard, S. Schmauder, D.B. Zahl, and A.G. Evans, *Effects of misfit strain and reverse loading on the flow strength of particulate-reinforced Al matrix composites*, Acta Metall. Mater. 40 (1992), pp. 3113-3119.

[2] M.E. Fitzpatrick, P.J. Withers, A. Baczmanski, M.T. Hutchings, R. Levy, M. Ceretti, and A. Lodini, *Changes in the misfit stress in an Al/SiC$_p$ metal matrix composite under plastic strain*, Acta Mater. 50 (2002), pp. 1031-1040.

[3] J. Orr and D.K. Brown, *Elasto-plastic solution for a cylindrical inclusion in plane strain*, Eng. Fracture Mech. 6 (1974), pp. 261-274.

[4] A.S. Argon, J. Im, and R. Safoglu, *Cavity formation from inclusions*, Metall. Trans. A 6 (1975), pp. 825-837.

[5] R.D. Thomson and J.W. Hancock, *Local stress and strain fields near a spherical elastic inclusion in a plastically deforming matrix*, Int. J. Fracture 24 (1984), pp. 209-228.

[6] A.A. Benzerga and J.B. Leblond, *Ductile fracture by void growth to coalescence*, Adv. Appl. Mechanics 44 (2010), pp. 169-305.

[7] R.W. Coade, J.R. Griffiths, B.A. Parker, and P.J. Stevens, *Inclusion stresses in a 2-phase alloy deformed to a plastic strain of 1%*, Philos. Mag. A 44 (1981), pp. 357-372.

[8] S.J. Harris, A. O'Neill, J. Boileau, W. Donlon, X. Su, and B.S. Majumdar, *Application of the Raman technique to measure stress states in individual Si particles in a cast Al-Si alloy*, Acta Mater. 55 (2006), pp. 1681-1693.

[9] A. Pyzalla, A. Jacques, J.-P. Feiereisen, T. Buslaps, T. D'Almeida, and K.-D. Liss, *In-situ analysis of the microstrains during tensile deformation of an AlSi-MMC at room temperature and elevated temperature*, J. Neutron Res. 9 (2001), pp. 435-442.

[10] A. Gangulee and J. Gurland, *On the fracture of silicon particles in aluminum–silicon alloys*, Trans. Met. Soc. A.I.M.E. 239 (1967), pp. 269–272.

[11] C.H. Cáceres, C.J. Davidson, and J.R. Griffiths, *Deformation and fracture of an Al-Si-Mg casting alloy*, Mater. Sci. Eng. A 197 (1995), pp. 171-179.

[12] J.-W. Yeh and W.-P. Liu, *The cracking mechanism of silicon particles in an A357 aluminium alloy*, Metall. Mater. Trans. A 27 (1996), pp. 3558-3568.

[13] T.R. Finlayson, J.R. Griffiths, D.M. Viano, M.E. Fitzpatrick, E.C. Oliver, and Q.G. Wang, *The partition of stresses in Al-Si-based metal-matrix composites*, Shape Casting: 2nd International Symposium: P.N. Crepeau, M. Tiryakioglu, and J. Campbell, eds. pub.TMS, Warrendale, PA, 2007, pp. 127-134.

[14] A. Baczmanski and C. Braham, *Elastoplastic properties of duplex steel determined using neutron diffraction and self-consistent model*, Acta Mater. 52 (2004), pp. 1133-1142.

[15] S. Cai, M.R. Daymond, and R.A. Holt, *Deformation of high β-phase fraction Zr-Nb alloys at room temperature*, Acta Mater. 60 (2012), pp. 3355-3369.

[16] B.M.B. Grant, E.M. Francis, J.Q. da Fonseca, M.R. Daymond, and M. Preuss, *Deformation behaviour of an advanced nickel-based superalloy studied by neutron diffraction and electron microscopy*, Acta Mater. 60 (2012), pp. 6829-6841.

[17] E.C. Oliver, M.R. Daymond, and P.J. Withers, *Interphase and intergranular stress generation in carbon steels*, Acta Mater. 52 (2004), pp. 1937-1951.
[18] B. Closset and J.E. Gruzleski, *Structure and properties of hypoeutectic Al-Si-Mg alloys modified with pure strontium*, Metall. Trans. A 13 (1982), pp. 945-951.
[19] C.H. Cáceres, C.J. Davidson, J.R. Griffiths, L.M. Hogan, and Q.G. Wang, *Hypoeutectic Al-Si-Mg foundry alloys*, Materials Forum, 21 (1997), pp. 27-43.
[20] C.H. Cáceres, C.J. Davidson, J.R. Griffiths, and Q.G. Wang, *The effect of Mg on the microstructure and mechanical behaviour of two Al-Si-Mg casting alloys*, Metall. Mater. Trans. A 30 (1999), pp. 2611-2618.
[21] Q.G. Wang, C.H. Cáceres, and J.R. Griffiths, *Damage by eutectic particle cracking in aluminium casting alloys A356/357*, Metall. Mater. Trans. A 34 (2003), pp. 2901-2912.
[22] T. Gnäupel-Herold, P.C. Brand, and H.J. Prask, *Calculation of single-crystal elastic constants for cubic crystal symmetry from powder diffraction data*, J. Appl. Crystallogr. 31 (1998), pp. 929-935.
[23] J.L. Tallon and A.J. Wolfenden, *Temperature dependence of the elastic constants of aluminum*, J. Phys. Chem. Solids 40 (1979), pp. 831-837.
[24] *EMIS Data reviews series 4: Properties of Silicon*. London: Institution of Electrical Engineers, 1988.
[25] Y.S. Touloukian, *Thermophysical properties of matter*, vol. 12 (Thermal expansion). New York: Plenum, 1975.
[26] J.R. Santisteban, M.R. Daymond, J.A. James, and L.J. Edwards, *ENGIN-X: a third generation neutron strain scanner*, J. Appl. Crystallogr. 39 (2006), pp. 812-825.
[27] S.F. Corbin and D.S. Wilkinson, *The influence of particle distribution on the mechanical response of a particulate metal matrix composite*, Acta Metall. Mater. 42 (1994), pp. 1319-1327.
[28] A.C. Larson and R.B. Von Dreele, *General Structure Analysis System (GSAS)*, Los Alamos National Laboratory Report LAUR 86-748 (2000).
[29] H.G. Priesmeyer, *The stress-free reference sample: Alloy composition information from neutron capture, in Measurement of Residual and Applied Stress using Neutron Diffraction*. M.T. Hutchings and A.D. Krawitz, eds. Kluwer Academic Publishers London, 1992, pp. 277-284.
[30] N. Shi, M.A.M. Bourke, J.A. Roberts, and J.E. Allison, *Phase-stress partition during uniaxial tensile loading of a TiC-particulate-reinforced Al composite*, Metall. Mater. Trans. A 28 (1997), pp. 2741-2753.
[31] G. Requena, G. Garcés, M. Rodríguez, T. Pirling, and P. Cloetens, *3D architecture and load partition in eutectic Al-Si alloys*, Advanced Eng. Mats. 11 (2009), pp. 1007-1014.
[32] J.D. Eshelby, *The determination of the elastic field of an ellipsoidal inclusion, and related problems*, Proc. Roy. Soc. London A241 (1957), pp. 376-396.
[33] M.F. Ashby, *The deformation of plastically non-homogeneous materials*, Philos. Mag. 21 (1970), pp.399-424.
[34] L.M. Brown and W.M. Stobbs, *The work-hardening of copper-silica. I. A model based on internal stresses, with no plastic relaxation*, Philos. Mag. 23 (1971), pp. 1185-1199.

[35] L.M. Brown and W.M. Stobbs, *The work-hardening of copper-silica*, Philos. Mag. 23 (1971), pp. 1201-1233.
[36] Y. Brechet, J.D. Embury, S. Tao, and L. Luo, *Damage initiation in metal matrix composites*, Acta Metall. Mater. 39 (1991), pp. 1781-1786.
[37] C.H. Cáceres and J.R. Griffiths, *Damage by the cracking of silicon particles in an Al-7Si-0.4Mg casting alloy*, Acta Mater. 44 (1996), pp. 25-33.
[38] M.R. Barnett, N. Stanford, A. Ghaderi, and F. Siska, *Plastic relaxation of the internal stress induced by twinning*, Acta Mater. 61 (2013), pp. 7859-7867.
[39] J. LLorca, J.L. Martínez, and M. Elices, *Reinforcement fracture and tensile ductility in sphere-reinforced metal-matrix composites*, Fatigue Fract. Engng. Struct. 20 (1997), pp. 689-702.
[40] J. Segurado and J. LLorca, *A computational micromechanics study of the effect of interface decohesion on the mechanical behavior of composites*, Acta Mater. 53 (2005), pp. 4931-4942.
[41] B. Wilner, *Asymptotic stress analysis of two phase materials*, Int. J. Eng. Sci. 33 (1995), pp. 127-130.
[42] B.J. Lee and M.E. Mear, *Stress concentration induced by an elastic spheroidal particle in a plastically deforming matrix*, J. Mech. Phys. Solids 47 (1999), pp. 1301-1336.
[43] A.J. Allen, M.A.M. Bourke, S. Dawes, M.T. Hutchings, and P.J. Withers, *The analysis of internal strains measured by neutron diffraction in Al/SiC metal matrix composites*, Acta Metall. Mater. 40 (1992), pp. 2361-2373.
[44] M.R. Daymond and M.E. Fitzpatrick, *Effect of cyclic plasticity on internal stresses in a metal matrix composite*, Metall. Mater. Trans. A 37 (2006), pp. 1977-1986.
[45] A. Roatta and R.E. Bolmaro, *An Eshelby inclusion-based model for the study of stresses and plastic strain localization in metal matrix composites. I: General formulation and its application to round particles*, Mater. Sci. Eng. A 229 (1997), pp. 182-191.
[46] W. Zhang, X. Dai, D. Ding, P. Gao, and M. Gu, *A monotonic loading approach for determining residual stresses of fiber reinforced metal matric composites*, Mater. Sci. Eng. A 616 (2014), pp. 29-34.
[47] R. Levy-Tubiana, A. Baczmanski, and A. Lodini, *Relaxation of thermal mismatch stress due to plastic deformation in an Al/SiCp metal matrix composite*, Mater. Sci. Eng. A 341 (2003), pp.74-86.
[48] J.J. Gilman, *Direct measurements of the surface energies of crystals*, J. Appl. Phys. 31 (1960), pp. 2208- 2218.
[49] J. Campbell, *Entrainment defects*, Mats. Sci. Technology 22 (2006), pp. 127-145
[50] J.R. Griffiths, *Commentary on 'Entrainment defects' by J. Campbell*, Mats. Sci. Technology 22 (2006), pp. 1001-1003.

Tables

Table 1. Physical and thermal properties of Al and Si.

	Temperature / K (˚C)	Young's modulus / GPa	Poisson's ratio	Coefficient of thermal expansion / 10^{-6} K^{-1}
Al	293 (20)	70.2	0.346	23.58
	357 (84)	67.5	0.351	24.20
	403 (130)	65.7	0.354	24.76
Si	293 (20)	162.7	0.223	2.55
	357 (84)	162.1	0.222	3.04
	403 (130)	161.6	0.222	3.25

Table 2. Lattice parameters a_0 for the NIST Si powder sample measured at 20°C.

Bank 1	Bank 2	NIST standard value
0.543014±0.000074 nm	0.543064±0.000059 nm	0.543119 nm

Table 3. Stresses in the Si inclusions at different temperatures under zero applied stress.

Temperature / °C	Measured stress / MPa	Calculated stress / MPa
20	–155	–155
84	–69	–65
130	–4	–7

Figure captions:

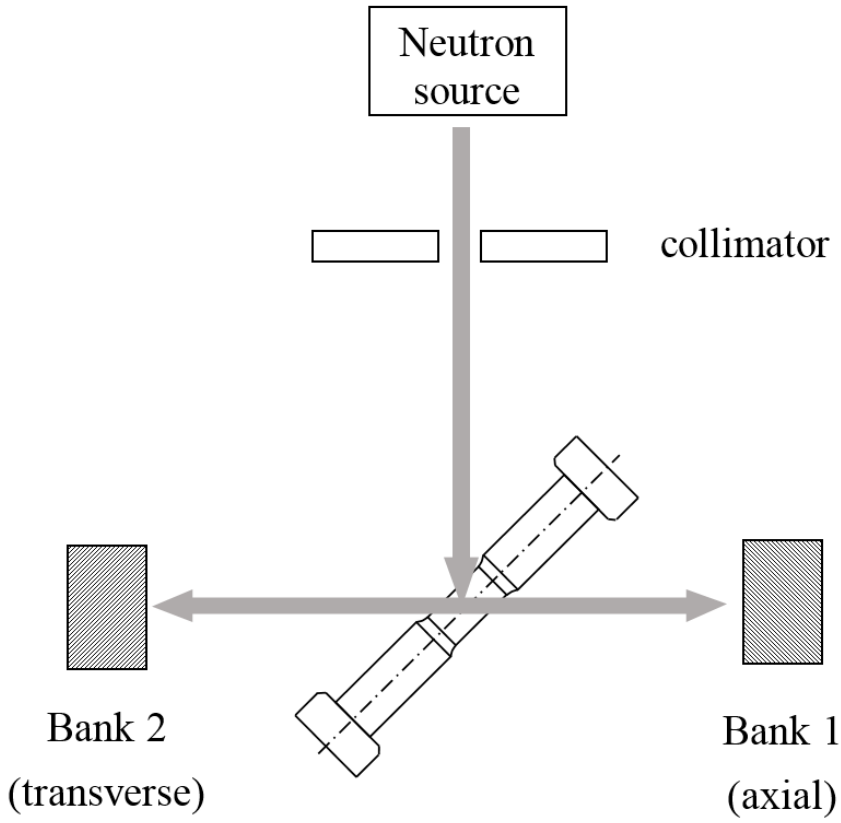

Figure 1. Schematic illustration of the experimental set-up at the ENGIN-X beamline at the ISIS facility. The neutron beam path and the design of the tension/compression specimens is shown and the specimen dimensions are given in the text.

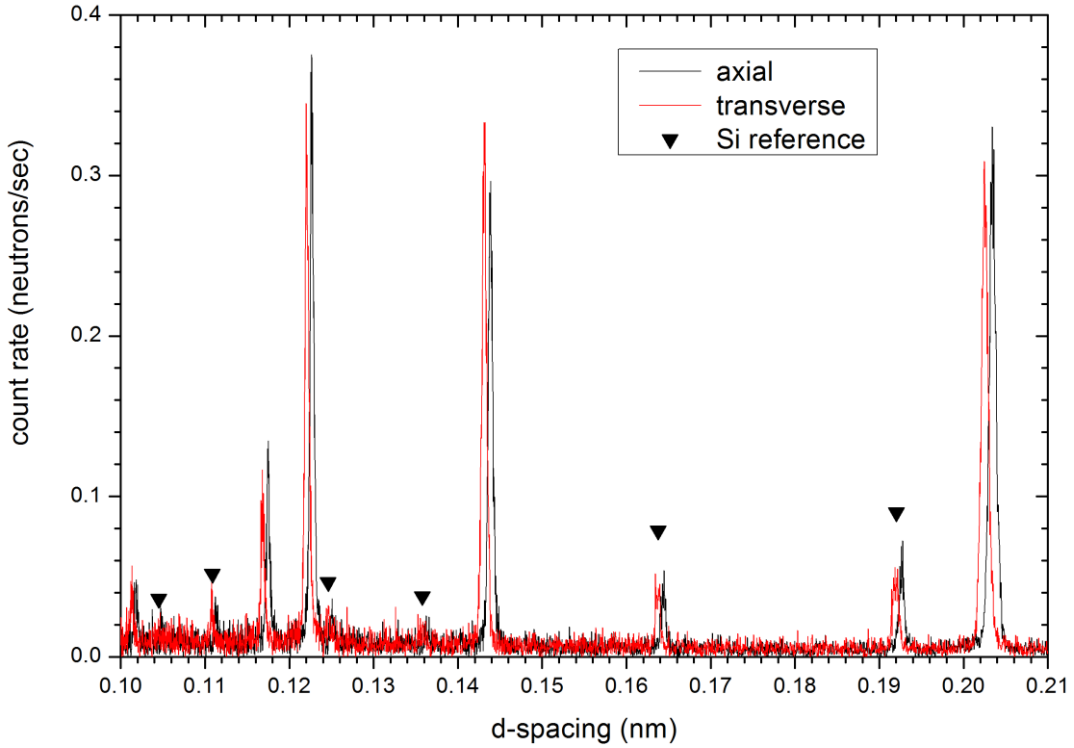

Figure 2. Sample diffraction patterns from the detectors measuring axial and transverse strains for the tension-first 20°C specimen. This example was chosen at maximum tensile load so that the spectra show maximum separation between banks.

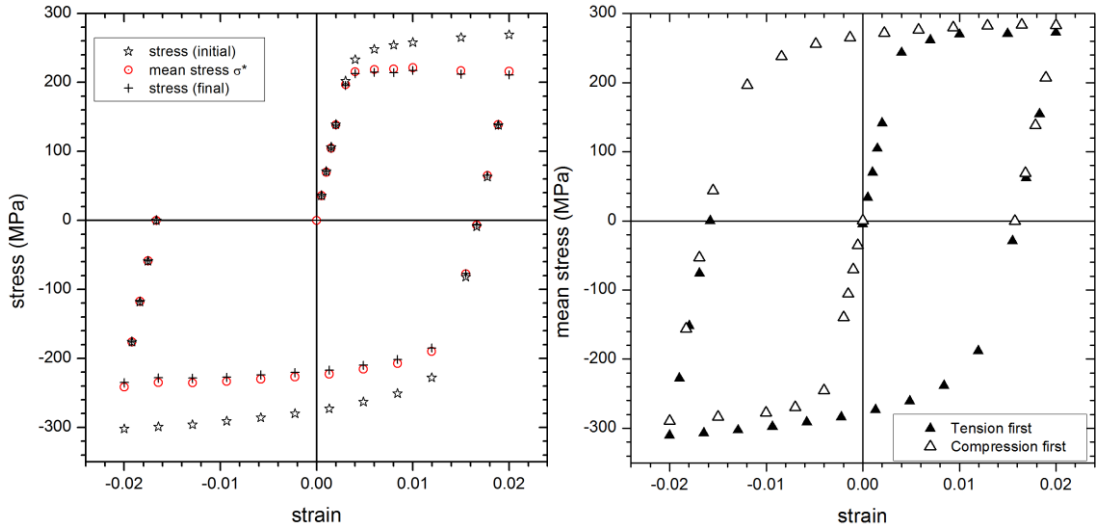

Figure 3. Stress as a function of total strain. (a) The 130°C test, showing the stress at the start and end of counting, and the mean stress defined in Equation 1; (b) The two 20°C tests (mean stress only); solid symbols for the test starting in tension and open symbols for compression-first.

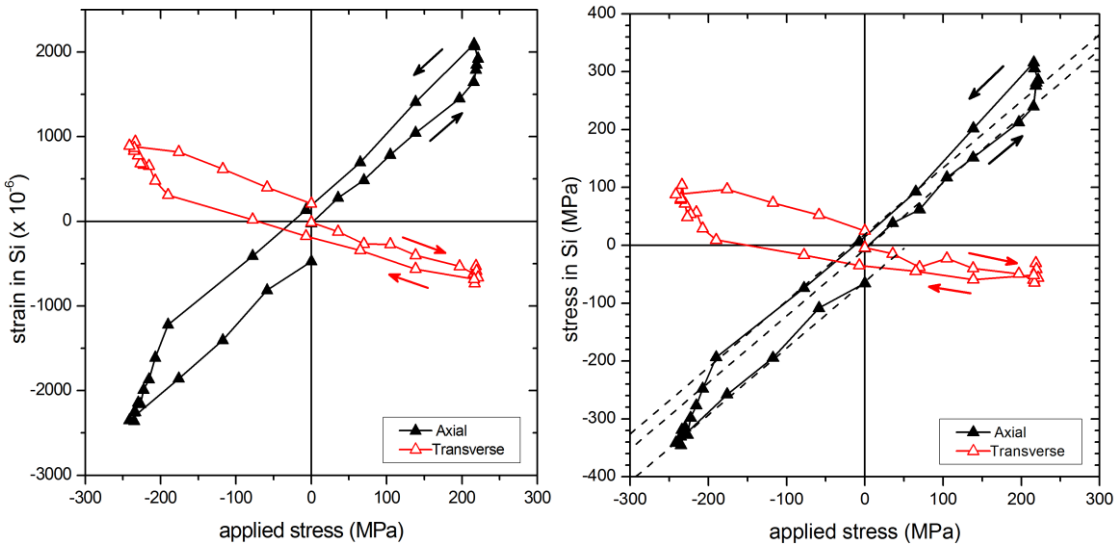

Figure 4. Tension-first test at 130°C. (a) Lattice strains, and (b) the derived stresses in the Si inclusions, as a function of applied stress. Closed triangles denote axial strains and stresses (parallel to the loading direction) and open triangles are the transverse values. The elastic lines for the initial loading and the final unloading are shown; their mean slope is 1.15 although the initial unloading has a steeper slope of 1.36. The plasticity stress, σ^{pl}, is the difference between the measured stress (solid lines) and the extrapolated elastic stress (dotted lines).

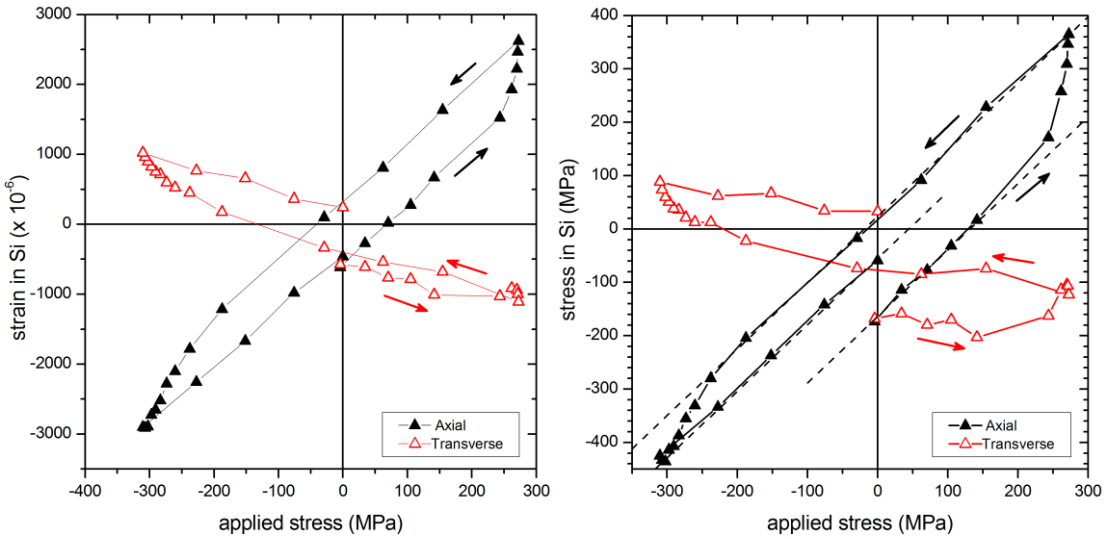

Figure 5. Tension-first test at 20°C: (a) Lattice strains, and (b) the calculated stresses in the Si inclusions, as a function of applied stress. Symbols as in Figure 4. The mean slope of the axial elastic loading/unloading lines is 1.25.

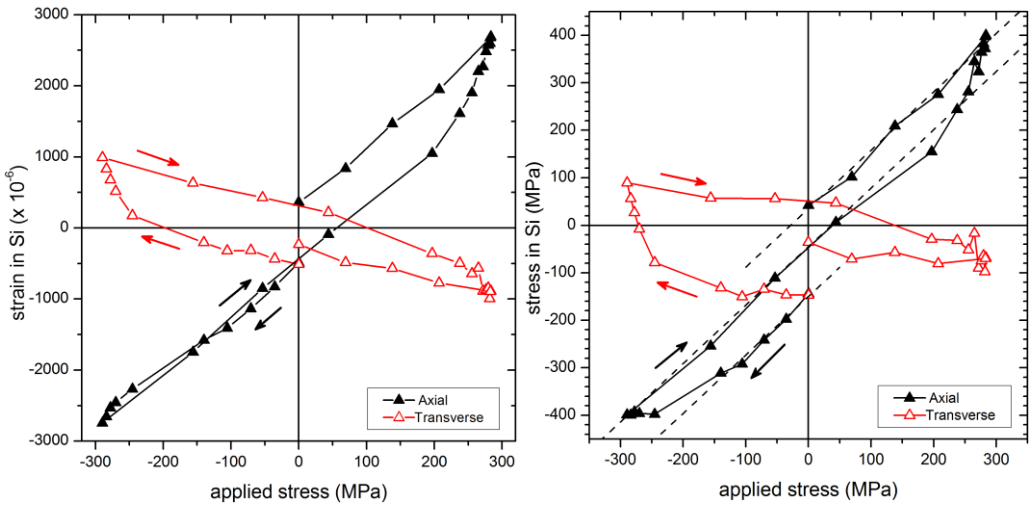

Figure 6. Compression-first test at 20°C: (a) Lattice strains, and (b) the calculated stresses in the Si inclusions, as a function of applied stress. Symbols as in Figure 4. The mean slope of the three axial elastic load/unloading lines is 1.23.

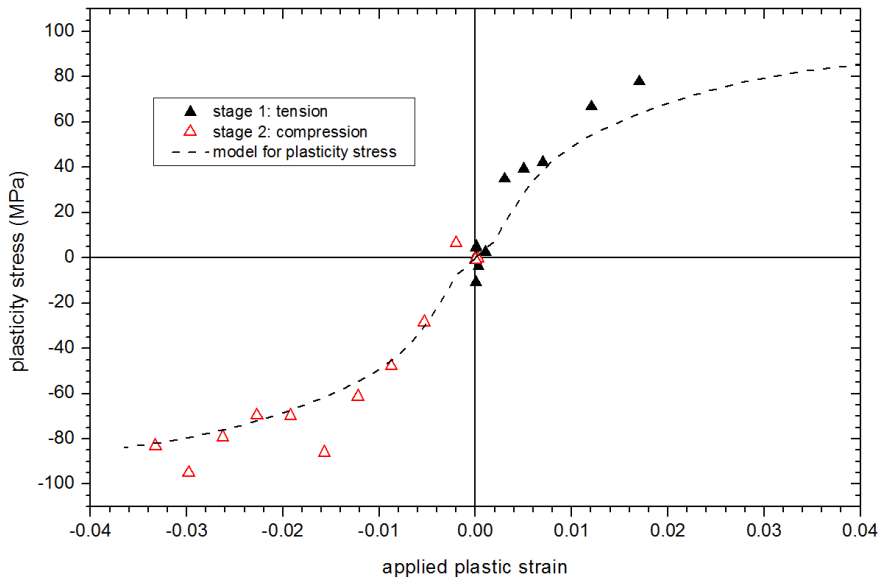

Figure 7. The development of a plasticity stress as a function of plastic strain at 130°C. Solid symbols are for tension and open symbols for compression. The compression results are offset from the zero load condition after unloading from the tension stage. The dashed lines are drawn from Figure 8 assuming tension/compression symmetry.

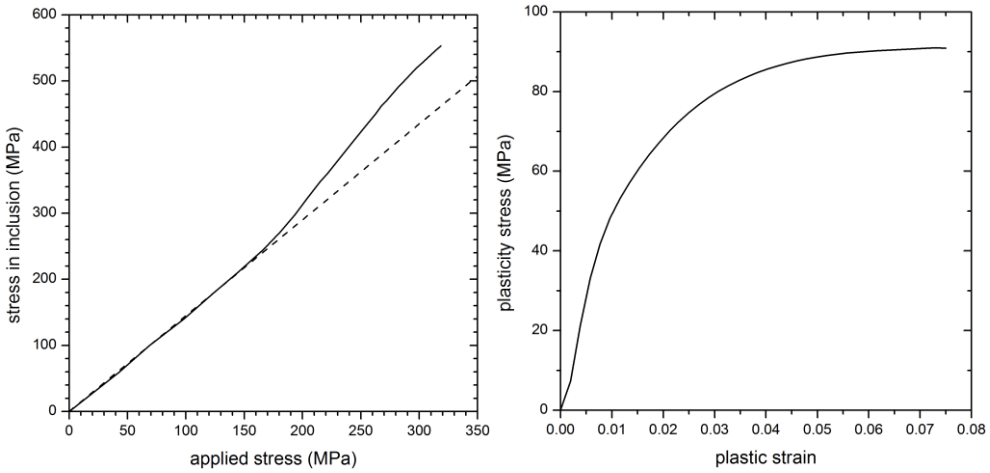

Figure 8. (a) The inclusion stress as a function of the applied stress. (b) The plasticity stress as a function of the applied plastic strain. Derived from data published by Segurado and LLorca [40].

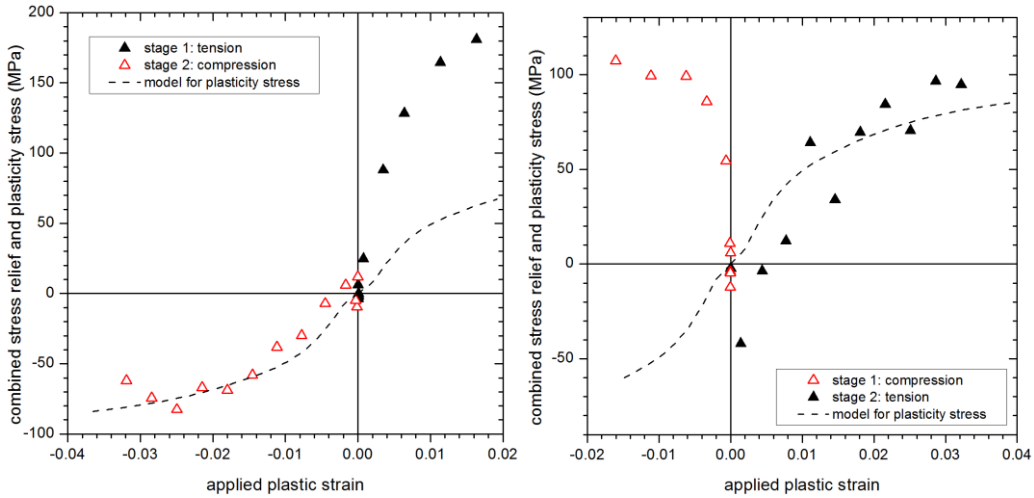

Figure 9. The development of an apparent plasticity stress as a function of plastic strain at 20°C. (a) The tension-first test. Solid symbols are for the initial tension and open symbols for the subsequent compression. (b) The compression-first test. Open symbols are for the initial compression and closed symbols for the subsequent tension. In both (a) and (b) the dashed lines are from Figure 8 assuming tension/compression symmetry.